IJESRT

INTERNATIONAL JOURNAL OF ENGINEERING SCIENCES & RESEARCH TECHNOLOGY
SYNTHESIS AND CHARACTERIZATION OF NICKEL DOPED ZINC OXIDE NANOPARTICLES BY SOL – GEL METHOD

Zafaran Abdul Fattah
Associate Professor, Deptt. Of Physics, Faculty of Education – Zingbar – Aden University

ABSTRACT
Zinc Oxide (ZnO) referred to as II – VI semiconductor because Znic belong to the second group and oxygen belongs to the sixth group of the periodic table. As grown ZnO in n – type semiconductor and its n – type conductivity can be controlled by growing it in an oxygen deficient atmosphere or by doping it with group III element like Al, Ga, or In. High quality 3d doped ZnO samples were required to synthesize a functional DMS (diluted magnetic semiconductor) whose magnetic properties were controlled by changing the carrier concentration, which Implies that there was a need to investigate the transport properties of (TM) ion doped ZnO. Hence the optical properties of undoped and TM ion Ni doped ZnO sample had been investigated and the valence state of these doped had been conformed through optical studies.

The chemical synthesis of semiconductor nanoparticles from (~1 – 20nm) in diameter with short – range structure were essentially the same as the bulk semiconductor.

For characterization of Nickel pure and doped Zinc Oxide $Zn_{11-x} Ni\ x\ O Zn_{11-x}Ni_xO$. ($x = 0.00, 0.01, 0.02, 0.03, o.o5$)nanopartical we used XRD and FTIR(Fourier transmission infrared) spectroscopy respectively.patterns reveal that the diffraction peaks of pure ZnO and nickel doped ZnO nanoparticles can be indexed to hexagonal wurtzite structure of ZnO which were in good agreement with the standard JCPDS file for ZnO (JCPDS36 – 1451, a = b = 3.249Å, c = 5.206Å). The grow size were calculated from XRD data was found that grain size decrease as Ni concentration increase up to 3% but decease up to 5%.

Spectrophotometry investigated the absorption of the different substances between the wavelength limits 190nm and 780nm.

The UV measurements pointed out that band gap energy decreases with the increase in Ni concentration by sol – gel method.(FTIR) of powder were recorded in the range 400 – 4000cm.

KEY WORDS: Zinc oxide crystal, nickel, X – ray diffraction, UV – v is spectroscopy, Fourier transform infrared, interferometer, detector, computer.

INTRODUCTION
Nanotechnology is the technology by which bulk materials reduced to nano - scale material and provided us an alternative way for device scaling. It is possible to arrange atoms into structures that are only a few nanometers in size, however nanostructure object possess intermediate size between molecular and microscopic (micrometer – sized) structures[1,2,3].

Zinc oxide (ZnO), a representative of II – VI semiconductor compounds, was a very versatile and important material. ZnO had a unique position among semiconducting oxides due to its piezoelectric and transparent conducting properties. It had a high electrical conductivity and optical transmittance in the visible region. ZnO had a wide band gap (3.37eV) and a large binding energy (60meV) and exhibited many potential applications in areas such as laser diodes, solar cells, gas sensors, optoelectronic devise. ZnO nanostructures had an active role to play in nano devices like nanogas sensors because the huge surface area enhances the gas sensing properties of the sensors[4,5,6].

High quality 3d doped ZnO samples were required to synthesize a functional DMS (diluted Magnetic semiconductor) whose magnetic properties are controllable by changing the carrier concentration, which implies that there was a need to investigate the transport properties of TM ion doped ZnO. Hence, the optical properties of powder of undraped and

TM ion Ni doped ZnO sample had been investigated. The valence state of those dopants had been confirmed through optical studies. The crystal structure and sample analysis using XRD and   FTIR spectroscopy respectively. The application of TM ion doped ZnO as UV absorber material had also been investigated in order to explore its application in ointments, creams and lotions to protect against sunburn and other damage to the skin caused by ultraviolet light[6,7,8].

The sol-gel process was a method of linked nanometer sized precursors in a solution or colloid to form a polymer when deposited. Regardless of the precursors material utilized in the formation of the sol gel, the material always shares the nano – pores that were characteristic of sol – gel materials. A colloid was a substance in which numerous suspended particles were small enough that they do not settle out of the liquid after a given amount of time, but were still enough that the particles do not dissolve. This suspension of nano – sized silicon particles becomes usable after draying at room temperature for a short time. During this time, the nanoparticales aggregate to form a highly porous solid, key to the sol – gel structure[10,11,12].

METHOD

Zink oxide was prepared from Zink acetate and Nickel Nitrate solution. 100ml of distilled water was added to it with addition of citric acid. The PH value of the solution reaches up to 1.5 to 2.0. Conventional heating experiment on temperature 40ºC were conducted on magnetic stirrer for 30 minutes.

In between the reaction ethylene glycol had been added for binding agent. After 30 min, ammonia was added drop wise until precipitation (ppt) occur. When the reaction were completed, the solid and solution phases were separated by centrifugation at 5000 rpm for 10min and the solid were free of salts with de – ionized water and ethanol. The separate gel from solution kept inside oven for 8hour for dry and evaporize the gases. Then grind it and made it in powder form .

Then a white color powder was claimed at 400ºC for 3 hours and then grind for uniformities of the powder.

The dry synthetic powders were weighted and the percentage yields were calculated from the excepted total amount of ZnO based on the solution concentration and volume and the amount that was actually crystallized.

The sample preparation has been done as shown in the block diagram (fig1). the various sample with different concentration (0%, 1%, 3%,5%) of Ni doped ZnO.
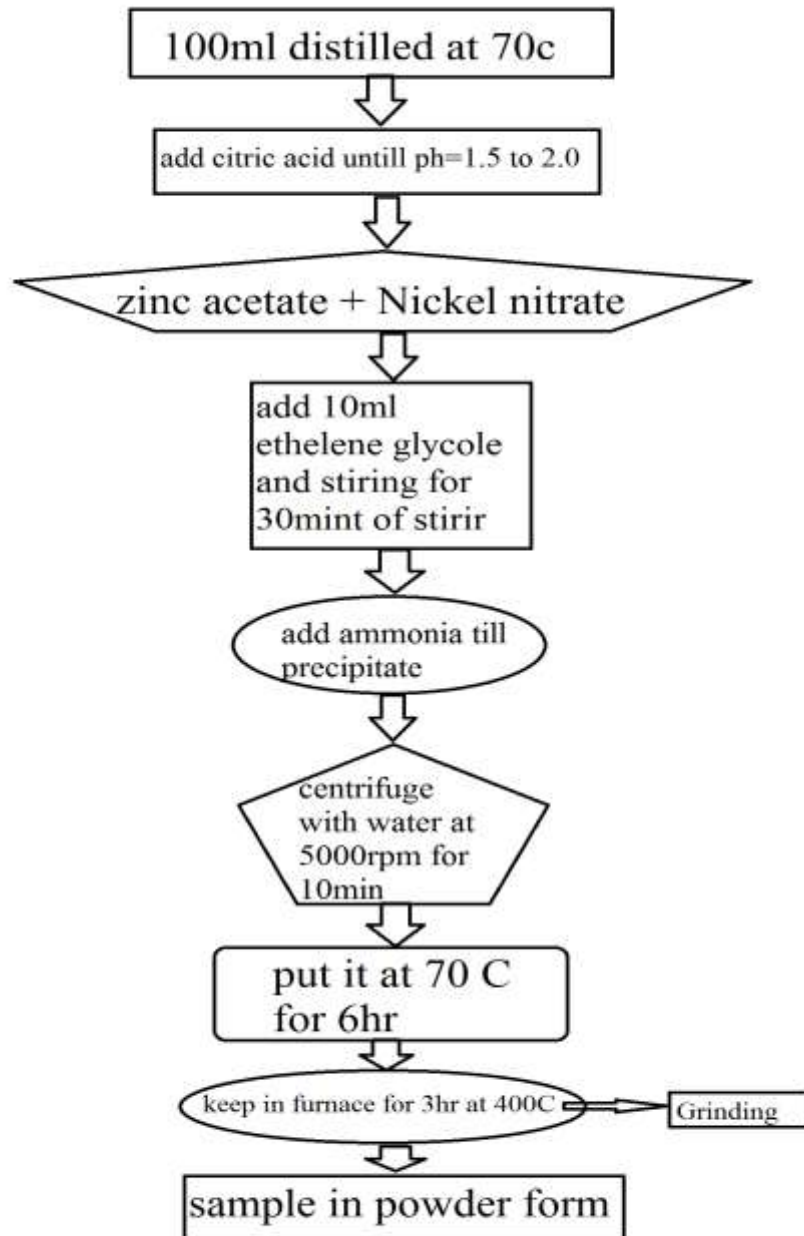
Fig1. The sample preparation .

RESULT AND DISCUSSION

The crystal structure and phase purity of as prepared undopedZnO and different composition of Ni–doped ZnOnanoparticales annealed at 400^{0}C were characterized using X – ray diffraction. Fig(2) shows a typical XRD pattern of pure ZnO and $Zn_{1-x}Ni_xO(x = 0.00, 0.01, 0.02, 0.03, o.o5)$nanopartical annealed at 400ºC XRD patterns reveal that the diffraction peaks of pure ZnO and nickel doped ZnO nanoparticles can be indexed to hexagonal wurtzite structure of ZnO which were in good agreement with the standard JCPDS file for ZnO (JCPDS36 – 1451, a = b = 3.249Å, c = 5.206Å) and the lattice parameters are listed in Table(1).
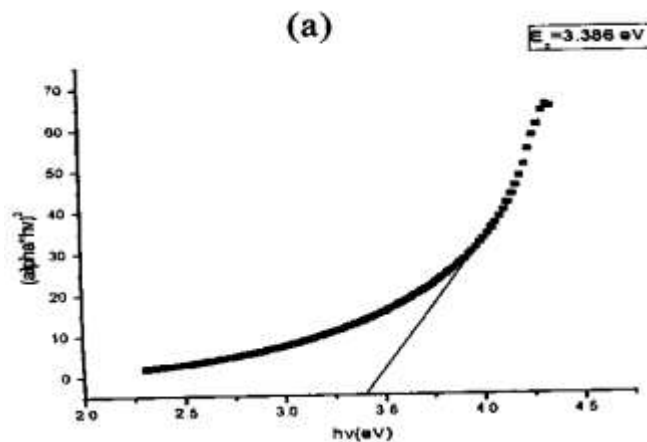
Fig . 2. Plots of (ahv)^{2}vs energy (hv) for sample with (a) 0%Ni

Fig 2.a. shows that the optical ban gap (EG) at 3.386ev, lattice constant (a=b= 3.279Å, c = 5.5182), the crystallite size of nanoparticales(D= 16.54nm) and FWHM(full width at half maximum) is 0.5009 with 0% of Ni doped
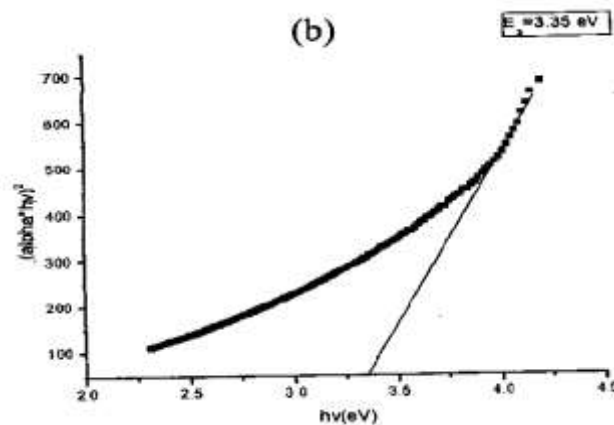

Fig . 2. Plots of (ahv)^{2}vs energy (hv) for sample with (b) 1%Ni

Fig2.b. shows the crystallite size (D= 13.82nm) with band gapEg(3.350ev), lattice constant (a=b= 3.279Å, c = 5.5182)and FWHM(full width at half maximum) of 0.6000with1%of Ni doped as well as the lattice parameters are gradually increases with increasing of Ni doping concentration in ZnO.
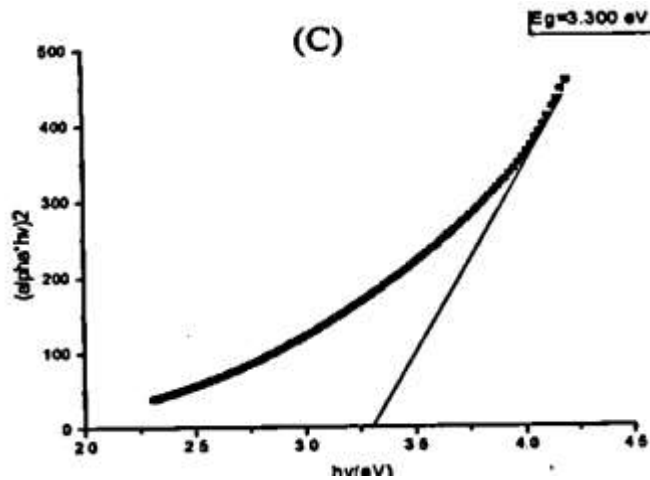
Fig . 2. Plots of (ahv)²vs energy (hv) for sample with (c) 3%Ni

Fig2.c. shows the crystallite size (D= 12.63nm) with band gap Eg(3.300ev) lattice constant (a=b= 3.279Å, c = 5.5182) and FWHM (full width at half maximum) of 0.6600 with 3%of Ni doped. As well as, the crystallite size is decrease with increase Ni doping concentration up to 3%.
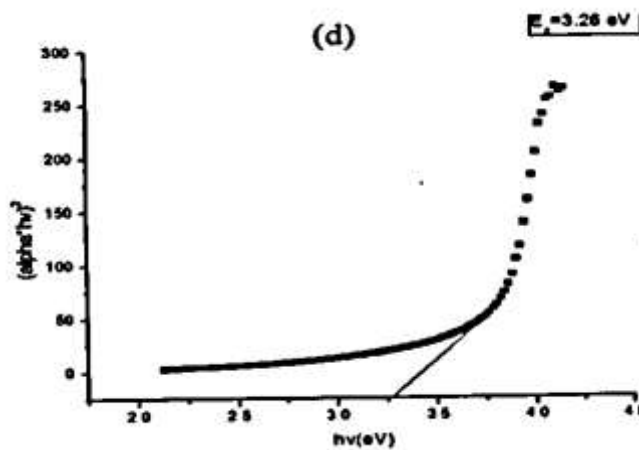

Fig . 2. Plots of (ahv)²vs energy (hv) for sample with (d) 5%Ni

Fig2.d. shows the crystallite size (D= 13.03nm) with band gap Eg(3.260ev), lattice constant (a=b= 3.279Å, c = 5.5182) and FWHM (full width at half maximum)of 0.6400 with 5%of Ni doped. Where the UV measurements pointed out that the band gap energy decreases with the increase in Ni concentration by sol–gel method.

The crystallite size of nanoparticles were estimated using Scherer's formula[5, 6, 16]

$$D = \frac{0.9\,\lambda}{\beta \cos \theta} \tag{1}$$

Where λ is the X – ray wavelength (Cu K_α = 1.5418Å), β was the full width at half maximum of the most intense peak and θ was the peak position[23,24].

As shown in Table (1), the crystallite size of the sample decreased with increasing Ni content up to 3% but in case of 5% concentration the crystallite size increase. Pure ZnO may be due to the annealing treatment of the samples at 400^0C. such variation in particle size was evident that pure ZnO exhibits broad diffraction peaks when compared to that nickel doped samples. Table (1) show that the lattice constant a and c of nickel doped ZnO nanoparticles were slightly larger than those of pure ZnO, because the ionic radius ofNi^{2+} (0.68Å) was larger than that of Zn^{2+} (0.60Å).

The UV – visible spectra have been shown in fig (3) which attributes that strong UV absorption was characteristic of all measured sample, which attains a plateau above 360nm. The optical band gap of the nanopowders was determined by applying the Tauc relationship as given below[32]:

$$\alpha h\upsilon \;=\; B(h\upsilon - Eg)^n \tag{2}$$

Where α was the absorption coefficient (α = 2.303A/t, here A was the absorbance and t was the thickness of the cuvett), B was the constant, h was Planck's constant, υ was the photon frequency, and Eg was the optical band gap. The value of n = ½, 3/2, 2 or 3 depending on the nature of electronic transition responsible for absorption and n = ½ for direct band gap semiconductor. The effect of Ni doping concentration on the band gap of ZnO and substitution of Ni^{2+} ions in tetrahedral site of wurtzite structure of ZnO was further confirmed using UV – visible optical spectroscopy measured in the range 200 – 700nm. The absorption band edge of undopedZnOis observed a 382nm and it gets shifted to longer wavelength region for the Ni – doped samples.

Table 1. the crystal size calculate from XRD data and band gap from UV of with different % of Ni doped.

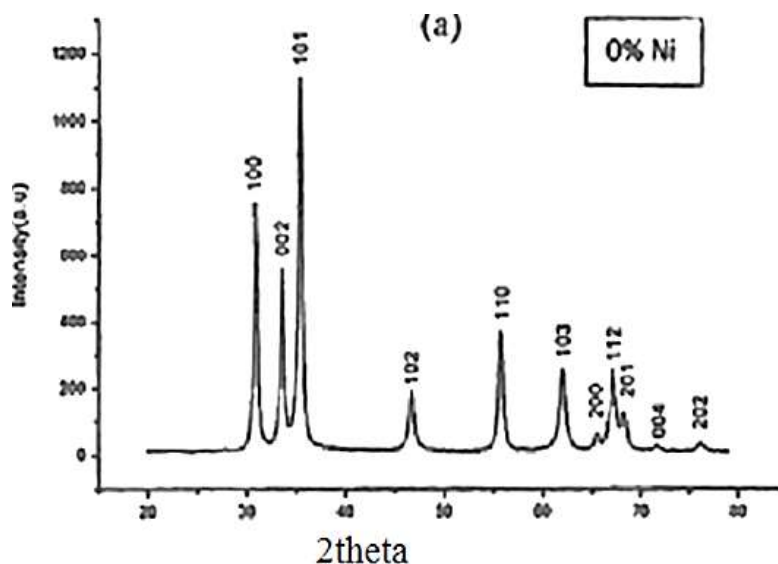| Ni conc. (%)	FWHM	D(nm)	E_g(ev)	Lattic constant(Å)	
				a = b	c
0	0.5009	16.54	3.386	3.279	5.182
1	0.6000	13.82	3.350	3.300	5.270
3	0.6600	12.63	3.300	3.302	5.2708
5	0.6400	13.03	3.260	3.340	5.280

Fig .3.a. X – ray spectra of Ni doped ZnO (a) 0%Ni, 2theta (diffraction angle)is the peak position vs intensity of sample

Fig 3. Shows a typical XRD pattern of pireZnO and Zn_{1-x}, Ni_xO for x = 0.00 nanoparticles annealed at 400C°, XRD patterns reveal that the diffraction peaks of pure ZnO and nickel doped ZnO, the intensity of NiO peak alternate increase with increasing nickel concentration indicating that phase segregation has occurred.
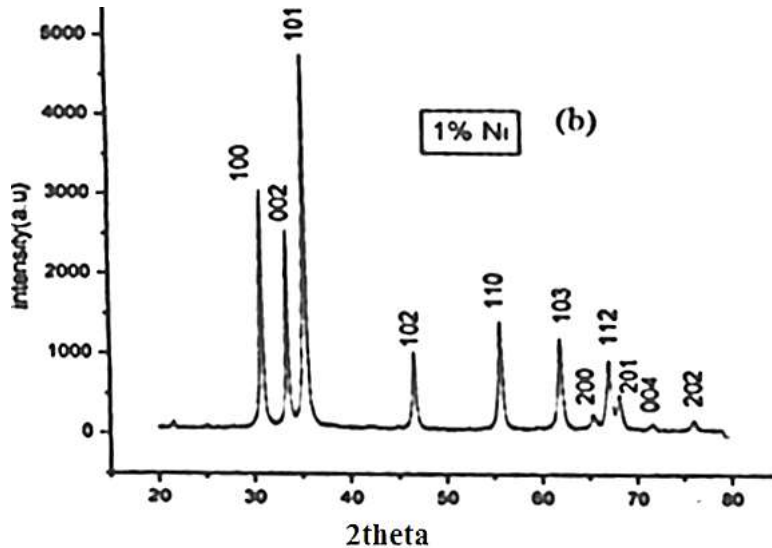

Fig .3.a. X – ray spectra of Ni doped ZnO (a) 1%Ni, 2theta (diffraction angle)is the peak position vs intensity of sample

Fig 3. Shows a typical XRD pattern of pure ZnO and Zn_{1-x}, Ni_xO for x = 0.01 nanoparticles annealed at 400C°, XRD patterns reveal that the diffraction peaks of pure ZnO and nickel doped ZnO, the intensity of NiO peak alternate increase with increasing nickel concentration indicating that phase segregation has occurred and the crystallite size of the sample decrease with increasing Ni content up to 3% but in case of 5% concentration the crystallite size increase.
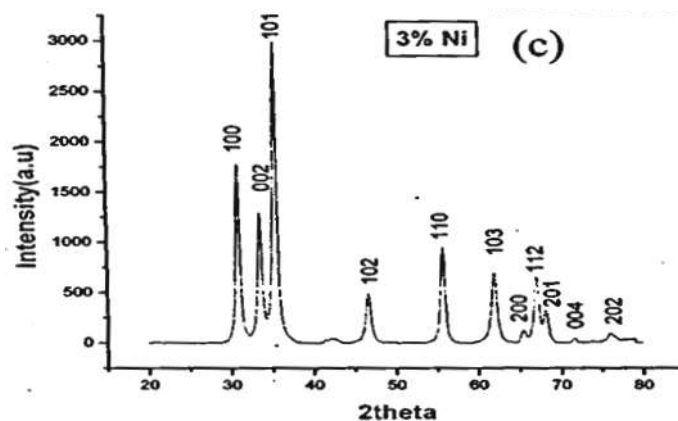

Fig .3.a. X – ray spectra of Ni doped ZnO (a) 3%Ni, 2theta (diffraction angle)is the peak position vs intensity of sample

Fig 3. Shows a typical XRD pattern of pure ZnO and Zn_{1-x}, Ni_xO for x = 0.03 nanoparticles annealed at 400C°, XRD patterns reveal that the diffraction peaks of pure ZnO and nickel doped ZnO, the intensity of NiO peak alternate increase with increasing nickel concentration indicating that phase segregation has occurred, the crystallite size of the

sample decrease with increasing Ni content up to 3% and the FWHM gradually increases the concentration of Ni in ZnO from 0% to 3% .
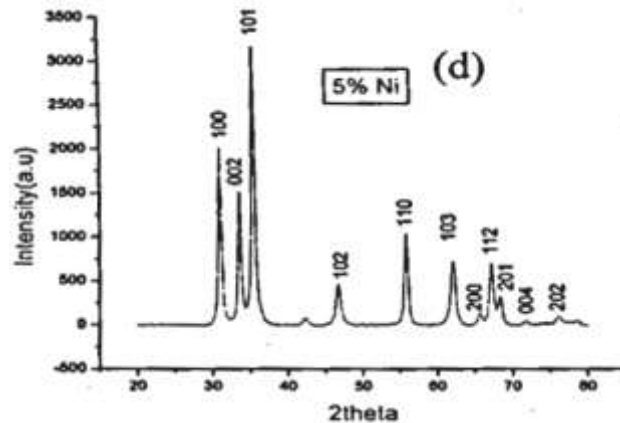

Fig .3.a. X – ray spectra of Ni doped ZnO (a) 5%Ni, 2theta (diffraction angle)is the peak position vs intensity of sample

As also evident in this graph as will that 5% concentaration of Ni the crystallite site increase annealed from that of as – prepared pure ZnO may be due to the annealing treatment of the sample at 400C°. such variation in particle size is evident that pure ZnO exhibits broad diffraction peaks when compared to that of nickel doped sample.

Change in the dipole moment of Ni–O bands in the ZnO:Ninanopowdre prepared by the sol – gel method is small leading to the weak absorption band around 779.65cm^{-1} in the fig (3c).

There was a sharp increase in absorption at energies close to the band gap that manifest itself as an absorption edge (or reflection threshold) in the UV–Vis absorption spectrum.For direct band gap of semiconductors can be calculated using the Tauc relationship:

$$\alpha h\upsilon = B(h\upsilon - Eg)^n$$

Where α was the absorption coefficient (α = 2.303A/t) here A was the absorbance and t is the thickness of the cuvette), B was constant, h was Planck's constant, υ was the photon frequency, and Eg was the optical band gap. The value of n = 1/2, 3/2, 2 or 3 depending on the nature of the electronic transition responsible for absorption and n = ½ for direct band gap semiconductor.

In infrared spectroscopy, IR radiation was passed through a sample. Some of the infrared radiation was absorbed by the sample and some of it was passed through (transmitted). The resulting spectrum represented the molecular absorption and transmission, creating a molecular fingerprint of the sample. Like a fingerprint on two unique molecules structure produced the same infrared spectrum. This made infrared spectroscopy useful for several types of analysis.

An infrared spectrum represented a fingerprint of a sample with absorption peaks which correspond to the frequencies of vibration between the bonds of the atoms making up the material. Because each different material was unique combination of atoms, no two compounds produce the exact same infrared spectrum. Therefore, infrared spectroscopy could result in a positive identification (qualitative analysis) of every different kind of material.

The addition weak band and shoulder as many be due to the higher Ni percentage. Absorption bands show the presence of resonance interaction between vibration modes of oxide ions in the crystal. The change in observed of bands may be due to ZnO – Ni stretching shown in fig (4).
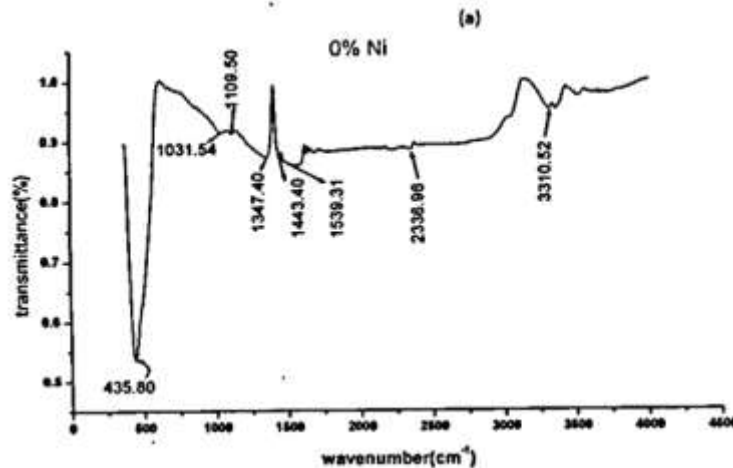
Fig 4. FTIR spectra of ZnO with concentration (a) 0%, (b) 1%, (c) 3%, (d) 5%

For x = 0.00 concentration in fig (4.a), the peak appeared at 3310.52cm indicates the presence of stretching vibration of the O – H group. The absorption peaks observed around $2336.96cm^{-1}$ were assigned to the Co_2 mode. The Co_2 mode were present in the FTIR spectra due to atmospheric Co_2 in the sample. Sample might had been trapped some CO_2 from the atmosphere during FTIR characterization which might had given such mode. The strong absorption band at $1539.31cm^{-1}$ is assigned to the C=O stretching. The strong absorption bending of the hydroxyl group at $(1347.40 – 1443.40)cm^{-1}$. The absorption band at $435.80cm^{-1}$ is assigned to the stretching mode of ZnO.
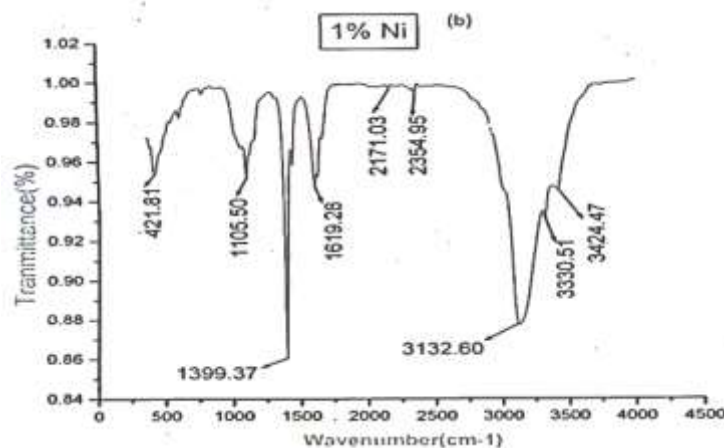

Fig 4. FTIR spectra of ZnO with concentration (a) 0%, (b) 1%, (c) 3%, (d) 5%

Spectra for x = 0.01 concentration in fig (4.b), the bands around $3330.50 – 3424.47cm^{-1}$ were assigned to the –OH mode to the strong bands associated with OH stretching vibration of H_2O in the ZnOnanocrystal.The presence of these bands may be due to atmospheric water during FTIR measurement. The presence of brand corresponding to acetate is clearly seen at $2354.95cm^{-1}$ and are assigned to CO_2. The strong absorption band at $1619.28 cm^{-1}$is assigned to the C=O stretching. Bands around $1105.50cm^{-1}$ are due to the characteristic frequency of inorganic ions. Bands around $1399.37 cm^{-1}$ are due to the oxygen stretching and bending frequency.
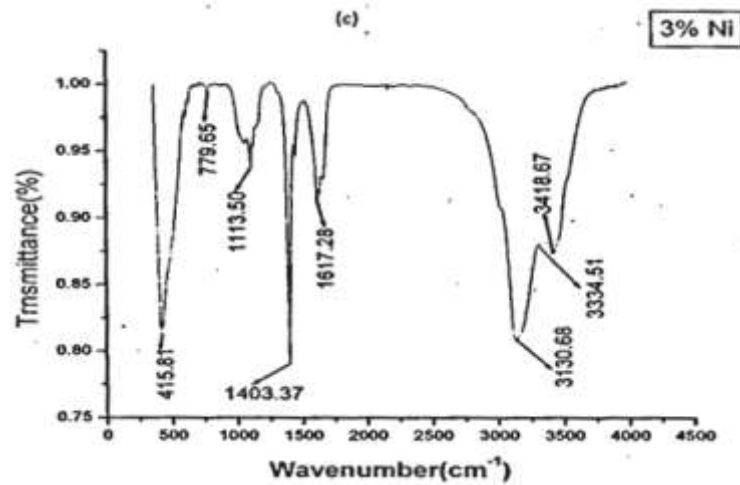
Fig 4. FTIR spectra of ZnO with concentration (a) 0%, (b) 1%, (c) 3%, (d) 5%

For x = 0.03 concentration in fig (4.c) the peaks are disappeared corresponding to acetate. The strong absorption band observed for the O – H stretching at (3334.51 – 3418.67) cm^{-1}. The addition weak bands and shoulder at 3334.51 – 3418.67cm^{-1} may be due to nano structure formation of the sample.
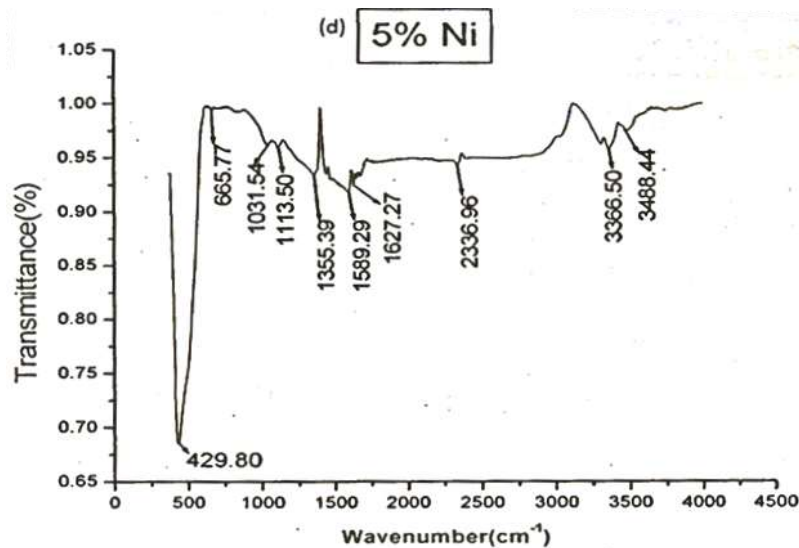

Fig 4. FTIR spectra of ZnO with concentration (a) 0%, (b) 1%, (c) 3%, (d) 5%

For x=0.05 concentration in fig (4.d) the band corresponds to acetate again present at 2336.96cm^{-1}. The hydroxyl group present at (3366.50–3488.44) cm^{-1} but not with broad spectrum which means less water content present at higher percentage Ni doped.

CONCLUSION

In synthesized nanocrystals of pure and Ni doped ZnO through chemical sol – gel method using citric acid as the fuel. The crystal structure of the Zn$_{1-x}$Ni$_x$O compound with x = 0.00, 0.01, 0.03 had been studied. From XRD data, it was conformed that all samples were in the wurtziteZnO structure. No secondary phases were observed for the simple

synthesis process for the Ni doped ZnO samples were shown in Fig(1). The XRD measurements suggest that Ni atoms substitute Zn sites in the crystal without changing the wurtzite structure. The lattice parameter 'a' and 'c' increase with the doping percentage of Ni increase which indicates that Ni substitute at the place of Zn. The grain sizes were calculated from XRD data. It was found that grain size decreases as Ni concentration increases up to 3% but in case of 5% Ni concentration the grain size increase.

Fourier transmission infrared (FTIR) spectra of the powders (as pellets in KBr) were recorded in the range of 400 – 4000cm^{-1}. Prominent IR peaks were analyzed and assigned.

REFERENCE

1. A.E Jime<<nez – Gonza, Jose A. Soto Urutera, R. Suarez – Parra Journal of Crystal growth 192 (1998) 430-438.
2. B.M. Keyes, L.M. Gedvilas, X. Li, T.J. Coutts Journal of Crystal Growth 281 (2005) 297 – 302.
3. C K Ghosh, S Malkhandi2, M K Mitra and KK Chattopadhyay IOP PUBLISHING J. Phys. D: Appl. Phys.41 (2008) 245113.
4. Element of Solid State Physics. J.P.Srivatava, second edition PHI learning Press.
5. H. Kim, A. Pique, J.S.Horwitz, H. Murata, Z.H.Kafafi, C.M.Gilmore, D.B.ChriseyThin Solid Film 377378_2000.798802.
6. Introduction to solid state physics, Charles kittel 7th edition, press JohniWiley &Sons.
7. Jinghua Jiang, Dawei He Yongsheng Wang, Ming Fu, Bin Feng, ChangbinJu. Yufan Du. IEEE proceedings of 16th IPFA – China.
8. K. J. Chen, T.H. Fang, F.Y.Hung, L.W.Ji, S.J.Chang, S.J. Young, Y.J.Hsiao Applied Surface Science, 254 (2008) 5791 – 5795.
9. Kazuki Yamauchi, KasilingamSenthikumar, Takahiro Yamamae and Yasuhisa Fujitta. Journal of Korean Physics Society, Vol.53, No.1, july 2008,pp. 46 – 49.
10. Pin – Chuan Yao, Shih – Tse Hung, Yu Shuan Lin, Wen – Tsia Yen , Yi Cheng Lin Applied Surface Science 257(2010)1441 – 1448.
11. R. Elilarassi, and G. Chandrasekaran. J Mater Electron (2011) 22:751 – 756.
12. R. Elilarassi, and G. Chandrasekaran. OPTOELECTRONICS LETTERS Vol. 6. No.1, 1 January 2010.
13. Ü. Özgüur, Ya. I. Alivov, C. Liu, A. Teke, M. A. Reshchikov, S. Doğan, V. Avrutin, S. –J. Cho, H. Morkoç; J. Appl. Phys. 98, 041301 (2005).
14. S. N. Bai, T. Y. Tseng, J. Appl. Phys. 74, 695 (1993).
15. M. Aslam, V. A. Chaudhary, I. S. Mulla, S. R. Sainkar, A.B. Mandale, A.A. Belhekar, K. Vijayamohanan, Sens. Actuators A-phys.75, 162 (1999).
16. O. Kluth, B. Rech, L. Houben, S. Wieder, G. Schope, C. Beneking, H. Wagner, A. Loffl, H.W. Schock, Thin Solid Films 351, 247 (1999).
17. N. K. Zayer, R. Greef, K. Roger, A. J. C. Grellier, C. N. Pannell, Thin Solid Film 352, 179 (1999).
18. S. J. Pearton, C. R. Abernathy, D. P. Norton, A. F. Hebard, Y. D. Park, L. A. Boatner, J. D. Budai, Mater. Sci. Eng. R 40, 137 (2003).
19. F. Pan, C. Song, X. J. Liu, Y. C. Yang, F. Zeng, Mater. Sci. Eng. R62, 1 (2008).
20. S. M. Haile, D. W. Johnson, G. H. Wiseman, H. K. Bowen, J. Am. Ceram. Soc. 72, 2004 (1989).
21. M. Andres-Verges, M. Martinerz-Gallego, J. Mater.Sci. 27, 3756 (1992).
22. C. H. Lu, C.H. Yeh, Ceram. Int. 26, 351 (2000).
23. X. Y. Kang, T. D. Wang, Y. Han, M. D. Tao, Mater. Res. Bull. 32, 1165 (1997),.
24. C. H. Lu, C. H. Yeh, Mater. Lett. 33, 129 (1997).
25. X. Y. Zhao, B. C. Zheng, C. Z. Li, H. C. Gu, Powder. Techonl. 100, 20 (1998).
26. J. Wang, L. Gao, Inor. Chem. Com. 6, 877 (2003).

27. R. Dogra, A.P. Byrne, M.C. Ridgway, J. of Electronic. Material 38, 623 (2009).
28. D. A. A. Santos, A. D. P. Rocha, M. A. Macêdo, Powder Diff Suppl 23, S36 (2008).
29. Th. Agne, Z. Guan, X. M. Li, H. Wolf, Th. Wichert, H. Natter, R.Hempelmann, Appl. Phys. Lett. 83, 1204 (2003).
30. S. Deubler, J. Meier, R. Schütz, W. Witthuhn, Nucl. Instrum. Meth. B 63, 223 (1992).
31. W. Sato, Y. Itsuki, S. Morimoto, H. Susuki, S. Nasu, A. Shinohara, Y. Ohkubo, Phys. Rev. B 78, 045319 (2008).
32. R. Dogra, A. P. Byrne, M. C. Ridgway, Optical Materials 31, 1443 (2009).